GEM TN-93-311

GEM Barrel Calorimeter Hadronic Modules

F. Lobkowicz
University of Rochester

May 5, 1993

Abstract:

We describe our plans for the design, manufacture and testing of the barrel hadronic calorimeter modules. We describe various feasibility and design tests, both those already completed and those still being performed. We discuss possible options, and chose among them those which seem to us most favorable.

GEM TN-93-311

The GEM Barrel Calorimeter Hadronic Modules

By F. Lobkowicz

University of Rochester

May 5, 1993

Abstract

We describe our plans for the design, manufacture and testing of the barrel hadronic calorimeter modules. We describe various feasibility and design tests, both those already completed and those still being performed. We discuss possible options, and chose among them those which seem to us most favorable.

1. Introduction

In this note we will present a first thorough discussion of the barrel hadronic calorimeter modules. We will outline the options we are aware of, we will present the reasons why we picked a certain option, or why we are deferring the choice awaiting some tests, calculations or cost estimates. We attempt to get down to the "nuts and bolts" issues of assembling and mounting the individual modules. While we cannot claim that this design is necessarily the final one, we want to present enough details that concrete criticisms and analyses by others can be made. In particular we request all people working on simulations to read the document carefully, and present soon any objections as to why there is not enough or too much material in some region. Anybody else is of course also invited to aim their arrows at any particular feature of the design.

This document summarizes the work of many people - too many to mention them all. So let me just thank the Rochester engineering group - Tom Haelen, Dan Spisiak and Dave Rocco - who either produced or checked all mechanical ideas. Paul Slattery helped with advice and management support. V. Radeka, S. Rescia and D. Makowiecki gave much input on matters electrical and electronic. The Martin-Marietta crew - Lyle Mason, *et al.* - not only produced the initial design concept, but also kept us honest during the whole design effort by criticizing ideas etc. D. Lissauer made sure that we received all relevant information from BNL. Kathy Hodel provided the many SPICE calculations discussed here. Ki-suk Hahn performed many mechanical and thermal studies. If this design is successful, much of the credit should go to these people. We have limited the number of actual authors to those who should be castigated for any mistakes, omissions or lack of clarity.

This is meant to to be a living document - to be upgraded as the design of the hadronic modules progresses. It is also supposed to introduce people joining the effort to the challenges and reasoning behind the design. We use a cylindrical coordinate system of r, ϕ and z. Here $z = 0$ is in the center of the central washer, that is at exactly 90° to the beams. This central plane is a symmetry plane for the barrel.

2. Modularity

The barrel calorimeter has to be built out of individual modules. With the advent of the Baseline II design, hadron calorimetry is limited to approx. the radial region between $R = 170cm$ and $R = 270cm$. Baseline II also prescribes lead as the preferred absorber material, and requires 4.5-5 λ in total absorption by the hadron calorimetry at 90°, with as much as possible being active absorber regions.

Very early on it had been decided that the the hadronic calorimeter should have a tower structure of approximately $\delta\eta \times \delta\phi = 0.08 \times 0.08$. In ϕ the division is quantized and the nearest possible value is $\pi/40 = 0.07854$. We will chose a $\delta\eta$ of the same magnitude. With this approach one hadronic tower covers exactly 9 EM towers, whose linear dimensions are three times smaller.

The above considerations, together with the need to read out each tower, require that each module be 0.1571 radians wide in ϕ; it thus covers two tower widths. The central support washer divides the barrel into two compartments in z; thus there will be $2 \times 40 = 80$ identical hadronic modules which make up one hadronic calorimeter layer.

There will be two module layers. On one hand one wants to minimize the number of such layers, since each carries with it some dead space for readout cables, tolerances, and support. On the other hand, at least two module layers are needed if one wants to prevent any ϕ-cracks extending over the full depth of the hadron calorimeter. In addition, additional stays are needed around $R = 230$ cm to tie the cryostat endwall to the central support washer (or alternately the two endwalls to each other); this is needed if the thickness of the endwalls is to be minimized.

Two hadronic layers allow a shift of the modules in each layer relative to each other by 4.5 degrees, thus eliminating any possible ϕ gap. One thus arrives at the arrangement shown in Figure 2.-1 We should stress here that the radial distances are not yet completely frozen. We are generally assuming that the barrel EM module stay ends at $r = 1679$ mm, and that the inner cryostat wall begins at 2674 mm. However, as of mid-February another set for these numbers was 1678 mm and 2707 mm, and one cannot yet assume all distances to be frozen completely. In any case, the total radial space allocated to hadron modules, including tolerances etc, is about 100 cm. In Figure 2.-1 we show an endview of one inner and one outer hadronic module. One should note the "stay" indicated in the drawing; this is a 5 cm diameter tube which connects the two end plates of the inner cryostat, and provides necessary stiffening. In addition, in at least one scenario the coolant ($LN2$ or LAr) will flow through this tube, carrying away the heat generated by the hadronic module preamplifiers.

Equally undetermined is the length of the modules. We are at present assuming a 25 mm thick central washer and an end to the Krypton volume at $z = \pm$ 192 cm in the region of the first hadronic layer. Some space is required to accommodate cables going from the EM detector to the feedthrus. Thus for the moment we assume that the first hadronic layer modules will have an overall length of 180 cm. An overall sideview of the modules inside the cryostat is shown in Figure 2.-2. In this drawing one also discerns that around $r = 210$ cm the cryostat changes shape to accommodate the feedthru bulkhead. The bulkhead itself is also the transition to the outer cylinder of the cold cryostat. This cylinder must be thickened near the ends, and this further constrains the space allocated to the hadronic modules. The outer hadronic module thus must be shorter, and one loses one half-cell (see below) near the end.

This arrangement also affects the assembly as will be discussed below.

3. The Cell structure - electrostatic transformers.

The calorimeter is in a magnetic field, and therefore one cannot use pulse transformers to change impedances between detector and amplifiers. The capacitance of one channel, on the other hand, is so large that one cannot simply readout all gaps in one tower in parallel. Thus we use an arrangement which has become known as "Electrostatic transformer". We illustrate this in Figure 3.-1. The detector consists of individual absorber planes, and in most of these planes the actual absorber is divided into tiles, where each tile has the size appropriate to one tower. Every sixth absorber plane is a solid absorber and is a ground plane.

Each of the tiles is electrically either floating (being held near ground by a large resistance) or connected to an amplifier. The electric field in the gap is provided by the outside pad on a 0.5 *mm* thick *G*-10 sheet which is shown in a blowup in Figure 3.-2. In a passive tile absorber layer, one pad is connected over a large resistance to ground and the other to HV. In the readout tile layer, which collects currents from both sides, both pads are connected to HV. This assures that there is in each gap an electric field pointing in the same direction, while no point is at a potential larger than the minimum required for a single gap.

The coupling capacitance between the individual pad and the tile adds another capacitor in series, which however never carries any ionization current. As discussed in Section 3.1, this leads to a reduction of the signal because each active krypton gap is followed by two passive gaps, each of which is only about 10 times larger.

3.1 Electrostatic transformers - simplified theory.

We do not want to assume that the reader is familiar with details of the concept of electrostatic transformer; we give therefore here a very simplified theory. This will be useful when we later discuss various constraints on the design and their effect on the readout signals.

Consider first N capacitors arranged in parallel as shown in Figure 3.-1a; they are tied to a power supply of constant voltage. We do not assume that their capacitances are equal, but label them as C_1, C_2, $\ldots C_N$. Each of these capacitors represents one gap in the liquid, and whenever there is ionization in the liquid, the capacitor "leaks", there is a current between the capacitor plates. If one such capacitor discharges internally some current I, then this current is simply supplied by the power supply (since the voltage has to stay constant). If more than one capacitor discharges, the net current supplied by the power supply is simply the sum over all the individual currents:

$$I_{tot} = \sum I_k$$

This picture is a simplified view of an arrangement where several gaps are connected to the same amplifier in parallel. It is an AC model; the DC high voltages are assumed to be connected through resistors large enough so as not to affect the currents on the scale of 10-50 nsec which we are discussing here. In this model one can consider the amplifier input as the power source of (nearly constant) voltage Vo and a source impedance equal to the amplifier input impedance of 10-20 ohm.

Now consider the same set of capacitors arranged in series, as shown in Figure 3-3b. If a current I_o flows in the $K-th$ capacitor, the voltages along all of the capacitors rearrange and therefore the power supply has to deliver only the current

$$I = \frac{\frac{1}{C_K} I_o}{\sum \frac{1}{C_j}} \quad . \tag{1}$$

where the sum goes over all capacitors, whether they actually "leak" or not. If many such capacitors carry a leakage current, the net current is simply the sum:

$$I = \frac{\sum_j \frac{I_j}{C_j}}{\sum \frac{1}{C_j}} \tag{2}$$

This is usually expressed by the simplified wording that in an electrostatic transformer the readout current is "the average of the currents in each gap, weighted by the inverse capacitance of each gap". Usually one assumes that all capacitors carry the same current. In our actual device, however, there will be "gap capacitors" which carry current, but also "blocking capacitors" which serve only to separate regions of high voltage from regions near ground, and thus carry no current. These blocking capacitors have typically a capacitance about ten times the gap capacitance, but there are five such capacitors in series with three active gap capacitors. This leads to a signal reduction of about 15%.

We stress that it is the inverse capacitance which matters. Should one of the capacitors have a capacitance very much larger than all the others, its effect on the net power supply current will be much smaller.

The denominator in Eq. 1 can be reinterpreted as the sum of only three inverse capacitances: the inverse capacitance of the $K-th$ capacitor with the current, the inverse of the net capacitance "below" and the inverse of the net capacitance "above". Indeed, in deriving Eq. 1 this is all one has to know - it is irrelevant how many individual capacitors produce these "below" and "above" net capacitances, and even whether these net capacitances are made up out of many capacitors or just one.

This helps us to discuss "Stray capacitances" as illustrated in Figure 3-3c: Two such stray capacitors are shown, one "above" and one "below" the capacitor whose current we are considering. The "below" capacitor will increase the current from the "power supply" (amplifier) since it increases the net capacitance below and thus reduces the inverse capacitance in the denominator in Eq. 1. In contrast, the "above" capacitor has to be considered as connected to a second independent power supply in our model. While the net current from both power supplies will increase if that capacitor is present, the current from the amplifier supply is reduced. The net effect of such stray capacitances is thus that the amplifier responds differently to the same current in each of the gap capacitors. Thus the detector cell acquires another inhomogeneity - the same ionization produced in different gaps produces a different response from the preamplifier.

Table 3.1.-1 Effect of blocking and stray capacitances. Amplifier response to a current pulse of 3.00 units in a single gap of a 3:1 transformer cell. The ideal system would respond with a current of 1.00. We use a "typical cell" with a gap capacitance of 183 pF.

Conditions	Response to current in		
	gap 1	gap 2	gap 3
No stray capacitances	0.86	0.86	0.86
Single tower, stray capacitance	0.69	0.81	1.07
Add neighboring 3/4 towers	0.83	0.85	0.92
Add neighboring 2/4 towers (end tile)	0.78	0.84	0.97

Of course, in reality these stray capacitances are only partially to ground; a larger fraction (typically 3/4) of the capacitance is to neighboring identical circuits which feed other amplifiers. By adding the signals from several neighboring amplifiers one can compensate for some but not all of this inhomogeneity. We have performed SPICE calculation to estimate the magnitude of the various effects. In Table 3.2.-1 we give the typical magnitude of these effects in the barrel hadronic modules. The output currents are all normalized to the current into the preamplifier from a given current in a single gap in the "ideal cell", where there are no blocking capacitors and no stray capacitances. When one looks only at a single channel, there is a 40% variation in the response to the same current in different gaps. This difference is much reduced if one adds the neighboring channels. For most of the tiles the effect is now about 10%, but larger in the end tiles which have ground on two sides.

3.2 Actual detector parameters.

Inside the barrel hadronic modules, the capacitance of a single gap varies between $C = 135\ pF$ at the inner end and first η bin of the inner hadronic layer to $C = 380\ pF$ at the outer end of the outer hadronic layer and at an η of 0.63 corresponding to $z = 180\ cm$. The ratio of the blocking capacitance to the gap capacitance is nearly the same for all tiles; it depends only on the thickness ratio and the ratio of dielectric constants of G-10 and krypton. The G-10 has a thickness of 25% of the gap; its dielectric constant of 5.0 is 3.05 times larger than that of LKr (1.64); thus a single blocking capacitor has a magnitude of about 12 times the gap capacitance. The nominal "loss factor" due to all the blocking capacitances in a single cell is then $3.00/3.5 = 0.857$, which agrees well with the SPICE estimate shown in Table 3.2.-1.

One can also estimate the "stray capacitance", which is is the capacitance between a single tile and neighboring tiles, or the nearby ground. Its ratio to the actual gap capacitance an be written as

$$\frac{C_{stray}}{C_{gap}} = 4 \times \frac{\epsilon_{(t)}}{\epsilon_{(Lkr)}} \times \frac{d_{gap}}{d_{tile}} \times \frac{thickness(tile)}{side(tile)}$$

Here ϵ are the dielectric constants of the LKr and of the material (t) between the individual tiles. The ratio of the distance d_{gap} of the LKr gap between absorber layers to d_{tile}, the distance between tiles in the same gap, also enters the expression. Finally the ratio of capacitances is also proportional to the ratio of the tile thickness to the tile side length.

As of today we have not found a material which could be inserted between the tiles and has a dielectric constant of less than 1.65, the value for liquid Krypton. We thus assume that LKr fills the material between tiles.

A single layer of tiles with the pad structure is shown in Figure 3-2. For most tiles 3/4 of the stray capacitance is to neighboring readout channels, while 1/4 of the capacitance is directly to ground. The exception are the first and the last tile in the eta direction, which have ground on two sides, and another tile on the other two sides.

The gap between tiles in an absorber layer wants to be as large as possible if one wants to minimize the stray capacitance. On the other hand, any gap creates a "hole" in the absorber material. In ϕ these gaps are projective through one layer, and thus one wants to be sure to minimize them. The smallest tile is 20.8 *cm* on a side. We want the gap to lose at most 1.5% of the active area, and this leads us to a gap width of 3 mm. In θ the gaps are nonprojective in a single cell, and so it makes sense to ask that such a gap never project to more than 1/2 cell depth. Since the innermost gap in η is at $\eta = 0.079$, $\theta = 4.5$ from the vertical, a 3 *mm* gap will produce a hole of depth

$$d = \frac{3\ mm}{tan(\theta)} = 3.8\ cm$$

or about half the cell depth of 7.3 *cm*. We are choosing a 3 *mm* gap width as a reasonable compromise between electrical performance (due to stray capacitances) and absorber loss by replacing absorber material by krypton. With these assumptions, the worst case stray capacitance per tile is 12% of the gap capacitance. Of course, in their overall effect these stray capacitances are (more or less) in parallel. As mentioned in the last section, stray capacitances produce an uneven response to the same current in different gaps in a single cell. Table 3.2.-1 shows the result of SPICE calculation, and demonstrates that with the parameters chosen the effect is not serious as long as one adds neighboring channels.

4. Absorber planes.

We define as a "plane" a single absorber layer separated by Krypton gaps from neighboring planes. Such absorber planes serve the dual purpose of interacting with hadrons and coupling the currents generated in the gaps to the amplifier inputs.

Throughout this discussion we will assume that the "basic" absorber for the hadron barrel calorimeter is lead. Lead was selected for the Baseline II design, but copper is a backup if it can be shown that there is no significant degradation in hadron resolution by using copper. For our purpose lead is the more difficult material; it is less rigid, and handling presents safety problems which will increase cost.

Each absorber plane has at both ends a notch which fits into a keyway on the endplates (see section 6.) Thus it is free to move radially, being restrained only by spacers which separate it from neighboring absorber planes by a 2 mm wide gap filled with LKr. The whole absorber stack is pushed together by a stack of Belleville washers hidden in the strongback.

There are three different types of absorber planes:

4.1 Ground plane:

This is a solid sheet of material 10 mm thick which extends through the width and length of the module. Even if lead is chosen in the end as basic absorber, we propose to use hardened copper or brass for the ground planes (Copper has slightly higher density, but it is easier to get brass of known hardness). Lead - even the hardest Calcium lead - will not withstand the pressure by the spacers which separate the individual absorber planes. Should it really become necessary to use lead, then it would have to be covered by a thin stainless steel sheet, or at least spacers would have to be made wider where they touch the lead. A further problem with lead is its large contraction during cooldown (0.6% compared to 0.4% for copper).

Before the final decision can be made, we will need detailed simulations to see how much using copper for ground planes changes the resolution and in particular the "constant term". In any case, the ground plane is electrically connected to the ground of the readout line (see section 5)

4.2 Tile planes.

4.2.1 Basic arrangement. The basic tile arrangement is sketched in Fig 4-1. The absorber (lead or possibly copper) is subdivided into individual tiles which cover approximately one tower. The individual tiles are exactly projective in ϕ, but within a single cell only the central readout tile has as its limits the well defined tower limits in η of $n\pi/40$. The other four tiles in the same cell then cover the same region in z. We chose such an arrangement for two reasons: (a) there is an advantage in having non-projective gaps between absorbers, and while in ϕ this is very difficult to achieve, in η it is a natural solution. (b) Spacers are required to keep the krypton gaps within tolerance. These spacers can now be purely radial in a single cell, making sure that there are no torques on the tile planes.

The tile arrangement is held together by two thin (0.5 mm) sheets of G-10. In the presently favored design the G-10 is copper-clad on one (the outer) side. This cladding is etched so that only pads of the same size as the underlying tile are left over. These pads are then connected by resistive ink, so that there is a resistance of 2-4 Mohm between any two neighboring pads. One of these pads is connected over a high resistance (again 2-4 Mohm) to ground, while the other has a similar connection to the high Voltage ($1.5 - 2.5\ kV$). One thus achieves an electrostatic arrangement as it is sketched in Figure 3-1.

4.2.1.1 Choice of resistor values. The resistor values between pads, while not very critical, are limited both from above and below. On one hand, the discharge current in the krypton gaps should not seriously change the voltage across the gap. Typical currents/tower in a gap are a fraction of a μA, and so resistances of the order of a few $M\Omega$ will lead to negligible voltage drops, but an increase by a factor 10 might begin to lead to voltage fluctuations. The lower limit is given by the parallel resistance noise in the amplifiers. Most pads are connected by three resistors to neighboring pads; there are six gaps/cell, and as many as 6 cells may be read out by a single amplifier. Thus each amplifier can see around 100 such resistors in parallel. Even with fast clipping one would want to keep the parallel resistance above 10-30 $k\Omega$; this suggests a lower resistance limit of 3 $M\Omega$. One also should note that resistive inks with high specific resistivity give less reproducible results, while inks with resistivity of a few hundred $k\Omega$/square require very thin lines if one wants resistances of more than 5 $M\Omega$.

4.3 Readout planes.

The readout planes are intrinsically identical to the tile planes, except that the tiles are connected to the signal lines going to the preamplifiers. Figure 4-2. is a sketch of these connections. Another difference is that on the tile planes both G-10 pads are connected to the H.V.; As illustrated in Fig.3-1, the readout absorber plane is the center plane of a cell, and collects currents from both sides.

4.4 Design variations of the G-10 construction.

Ideally the capacitance between the copper pads on the G-10 and the tile should be infinite. In actuality it is only 12 times larger (factor 4 from thickness, 3 from diel. const.) than the gap capacitance itself.

This capacitance is in series with the gap capacitance as far as charge collection is concerned, and makes the effect of the stray capacitance that much more serious. To increase this capacitance, one would want to make the G-10 thinner; but then the cover sheets become too thin to support the tiles as a reasonably rigid structure. There are two ways one could try to improve the situation:

1) Rely on the spacers and less on the rigidity of the tile absorber structure for keeping the assembly straight. Then one could consider making the G-10 only 0.25 mm = 0.01" thick. We will have to build a complete tile structure to check whether this option is feasible. One would also have to test each G-10 board to ensure that it will withstand the High Voltage; such thin sheets are often marginal in this respect.
2) Another way to increase this coupling capacitance is to use 0.5 mm thick G-10, but copper clad it on both sides. One etches identical pads on both side, and connects them through the G-10 itself. There is no need to use real throughplated holes; once a hole is punched, the two sides can be connected with conducting ink, conducting epoxy, or even soldered through the hole, since the material is so thin. Once such a connection is achieved, one separates the G-10 from the tile with a Kapton sheet which better withstands the HV. This could be made as thin as $0.1 - 0.2$ mm. The problem with this solution is the additional cost to produce the conducting connections between the two sides of the G-10, the kapton, additional assembly steps etc.

   We have done only rough estimates which we summarize here. The G-10 for the two sides of a single tile plane costs 88$ in medium quantities (140 planes and up); machining the pads, and silksreening on the resistors, adds 100$ to the cost if the machining is done on the Fermilab Gerber machine. If one needs double sided G-10, and has to machine both sides, and has to electrically join both sides, then this can be done either by throughplated holes (VERY expensive for these large sheets), or a labor intensive manual connection which would add about 100$/absorber layer to the cost. One then requires another step - inserting a Kapton sheet (about 60$/tile plane) and a few more gluing steps (say 30$/plane). Thus one would increase the coupling capacitance by a factor 3-5 at an additional cost of 200$/plane, or 6000$/module. We believe that the additional cost does not justify the small (12-14%) increase in signal amplitude.

4.5 Stray capacitance between tiles.

The stray capacitance between a tile and a neighboring tile - or ground - is proportional to the dielectric constant of the medium in between. It would therefore be advantageous to reduce the dielectric constant by introducing some special material. Unfortunately, the $\epsilon = 1.65$ of pure krypton is so low that it is difficult to produce any solid material with a lower ϵ. We are presently experimenting with "Microspheres", small (70 μ) hollow glass spheres which are used by industry as filler material to reduce the density (and ϵ) of constructs made of epoxy. Results so far are not encouraging; one would need a composite of about 90% microspheres and 10% epoxy in order to get the dielectric constant down to 1.5. Even with the lowest viscosity epoxy tried, such a mixture is so stiff that we were unable to achieve consistent mixing and curing. We are continuing with our investigations, but are assuming that the "material" between the tiles will be LKr.

4.6 Massless gaps.

There is extra "dead" material between the EM calorimeter and the inner hadronic modules, and a similar amount of passive absorber between the inner and outer barrel hadronic modules. Some of this space is necessary for strengthening the inner cryostat vessel, some is required for the EM amplifiers and cabling, and some must be allocated to take up tolerances. The structure of the hadronic modules themselves also requires some additional material at the inner and outer surface.

This amount of passive absorber should be compensated for by reducing the absorber thickness in the gaps immediately following the additional "dead absorber material". If one tries to equalize dE/dx, then one would remove substantially all the absorber from the first two "tile absorber" layers, an easy modification. The exact composition of the massless gaps will depend slightly on the main absorber material - copper or lead. The drawings in this document do not yet reflect this proposed change; they conform to the "baseline design" which has no massless gaps in the barrel hadronic modules. However, we definitely propose that this change be made in the design.

Introducing these massless gaps reduces the total absorber material in the hadronic modules. Some of this loss would be welcome to us, since we have had to shave the space allocated to tolerances. However, $4 \times 9\ mm = 3.6\ cm$ would be much more than we need; we plan to increase the thickness of each ground and tile plate to compensate for this loss. Note that this increases the nominal absorber thickness of $9\ mm$ by less than $0.5\ mm$.

4.7 Alternate absorber layer arrangement.

The hadronic modules in the endcaps are very large, and they have all their plates vertical. Significant cost savings can be achieved there by making the absorber layers coarser, while keeping the readout scheme similar. The comparison is made in Figure 4-3: the "standard scheme" has all readout planes of the same thickness. The "coarse scheme" has a $2.5\ cm$ thick ground plane, and the readout plane has tiles which are also $2.5\ cm$ thick. In between are the passive "tile" planes, which are made only out of a $0.85\ mm$ thick G-10 sheet, with the HV on one side (connected through a high resistance), while the other side is a "high resistance ground". There are several advantages to this system, and it should be seriously analyzed as an alternative:

1) There are a factor 5 fewer tile planes to be made; the ground absorber plate is thick enough that it could become a mechanical stiffener. This would lower overall costs.
2) The stray capacitance between neighboring "tiles" (actually pads) on the G-10 boards is very small (*ca* $10 - 15\ pF$). The main stray capacitances is between the (now very thick) readout tiles. This would make their effect more equal for all the readout gaps.
3) A small sacrifice in depth would allow 4:1 transformer ratio with no increase in the stray capacitance. This would increase the signal to noise ratio.

We do not advocate this modification if lead is used; if one wants to properly sample the EM showers produced by $\pi^0 - s$, one should limit a single layer of passive absorber to a maximum of 2 radiation lengths. This would not be true for lead (1 r.l. $= 5.6\ mm$), but is clearly satisfied with copper (1 r.l. $= 14.3\ mm$) even at a layer thickness of 2.5 *cm*. However, if we use copper as the main absorber material, the cost savings may warrant the small loss in resolution.

5. Connection to the preamplifiers - mother boards.

The capacitance of a single readout cell is $200 - 250\ pF$ on the average. Individual cells are spaced by $83 - 110\ mm$. When one considers a readout cable tying several of such cells together, then the capacitance of the cell has to be added to the actual cable capacitance when calculating the propagation time:

$$t = \frac{d}{v} = \sqrt{(\mathcal{L}C)}$$

For an ideal cable $\mathcal{L}$ and C are the total inductance and capacitance of the cable. Of course, the incident particles also move with the finite speed c, and since our signal pulse travels in the same direction, there is a partial compensation[1].

In our case the total propagation distance d all the way up to the amplifiers is at most $50 - 60\ cm$ at 90 degrees (in the outer layer), and $70 - 90\ cm$ at the ends of the hadronic barrel modules. In a kapton flat cable ($\epsilon = 3.4$) this corresponds to a propagation time of 3 nsec at 50 *cm* to 5.5 nsec at 90 *cm*. In a cable with a total distributed "parasitic" detector capacitance Cd in parallel, the impedance will be lowered and the transit time lengthened by the same factor

$$F = \sqrt{(1 + C_d/C_o)}$$

where C_o is the bare cable capacitance, which in Kapton for a cable length of 1 meter is

$$C_o = \frac{6150\ pF/m}{Z(ohm)}$$

This is to be compared with a detector capacitance of

$$C_d = 6 \times (200 - 250pF) = 1200 - 1500\ pF.$$

If it was a question of signal speed alone, one would like to have the ratio C_d/C_o to be much less than unity. However, the added capacitance also increases the noise which is proportional to the total capacitance of cable and all the cells. We chose $Z = 7$ Ohm, so that the cable capacitance is less than half the detector capacitance. Apart from lengthening the transit time, the individual detector cells also produce different time delays for the charge detection, since some of the collected charge starts out in the wrong direction. Depending on the statistical variations of the hadronic shower development, this can lead to a pulse shape which varies with the shower development in the detector. We are severely shaping (clipping) the output pulse, and the measured signal will depend on the arrival time of the charge at the preamplifier. Thus this effect will degrade the energy resolution. (The net integrated charge is of course always measured exactly). Figure 5-1 shows an idealized arrangement of 6 detector cells connected to an output line of well defined impedance. Figures 5-2a-f show the pulse shape as it would be measured at the output of a preamplifier with a risetime of approx. 10 nsec (RC=4 nsec) in an extreme situation where only one of the cells delivers all the charge. These figures were obtained using SPICE, and they show that with a 10 nsec risetime the variations in pulse shape are moderate but not negligible.

5.1 Readout cable - mechanical arrangement.

The readout cables will be kapton flat cables. One cable will read out two neighboring tiles, and for the inner hadronic modules it will read out two layers in depth. The cable will be attached to the individual readout tiles or ground planes by pins which fit into sockets mounted into the tiles. Figure 4-2 shows the conceptual design of a portion of the barrel inner hadronic module cable. The pins themselves are soldered to throughplated holes in the kapton cable using a low melting solder so as not to damage the kapton. Figure 5-3 shows the connection of an individual pin to the cable.

We prefer this design to an older one, where the connection was made by a screw instead of a pin. The usual commercial sockets have springs in them which allow for a moderate amount of misalignment between pin and socket - in our case between cable and tile - without any connectivity problems. One can also assemble the cable "on desktop" and the individual pins then are really a distributed connector.

6. Mechanical stability of a single module.

Each module is structurally a box, with the absorber and readout planes allowed to move inside, but constrained by spacers and Belleville washers. The box consists of a "strongback", a "bottom plate" and two "end plates" with the residual two sides of the box covered by a stress carrying "skin". All of these are made of freemachining brass (70:30), which has a thermal contraction between room temperature and $LN2$ temperatures very similar to that of Aluminum (relative length change is 0.03%). Figure 6-1 identifies these structural components. We note that the skin is a 0.5 mm thick sheet of brass, attached to to strongback, bottom plate and endplates by screws spaced approx 2.5 cm apart. There are a total of 80 such boxes in each hadronic layer - 40 on each side of the central washer.

The box has dimensions which are different for the inner and outer hadronic barrel layers, and the mass of a single modules also depends on whether lead or copper is being used as an absorber. Table 6.1.-a gives the approximate parameters for the two layers.

Table 6.1.-a Approx. Mechanical Parameters of a single module

	length (cm)	width (cm) outer	inner	weight (kg) copper	lead
inner hadronic	180	34	27	2000	2400
outer hadronic	147	35	42	2200	2600

The individual modules are supported at both ends. An inner hadronic module is supported by the washer and the endplate of the cold vessel. The outer hadronic modules are still supported by the central washer on one end, but on the other end there is a special ring support which is attached to the inner bulkhead only after most connections were made to the feedthrus in the bulkhead.

The orientation of each module is different, and so one has to check the mechanical stability of the arrangement in any orientation. A keyway in each endplate of a module connects fixes its position in ϕ relative to the support structure. Indeed, in this direction the module is exceptionally stable. The wide strongback and bottom plate keep the overall assembly rigid, and furthermore each of the absorberplanes inside is attached directly to the endplates via its own keyway. Thus each absorber plane supports itself from the endplates.

Radially each module is pinned at each end to the supporting structure - washer, cryostat endplate or support ring. At the washer end the pin restricts also the module from moving in the z-direction (parallel to the beam). At the other end the pin must be a sliding pin to accommodate the small (1/2 *mm*) shrinkage during cooldown. These pins give the total support for the top and bottom modules, and it is these modules which experience the largest deformations which would be much too large if there were no skins. These "skins" are necessary for the mechanical stability of the module, and their attachment to the various endplates (strongback, bottom plate) is crucial. The skins have holes punched at 2.5 *cm* intervals, and the brass around the holes is deformed so that it fits into the countersink of the hole in the endplate as shown in Figure 6-2. We use selftapping flathead screws to attach the skins.

6.1 Mechanical tests performed and planned.

6.1.1 Test of skin attachment. We have tested the idea of attaching the skins to the plates on a setup where a 0.5 *mm* thick, 30 *cm* wide brass sheet was mounted by screws spaced 25 *mm* apart in the manner described in Figure 6-2. Strain gauges at various places on the sheet measured local strain. One of the gauges was mounted 0.5 *cm* away from one of the screws along the direction of the pull; it showed only a small ($<$ 10%)increase in local strain. Up to a mean stress in the material (far away from the screws) of 10,000 psi = 7.0 $kg^*\ mm^2$, corresponding to a linear force of 208 pounds/inch along the edge, no permanent deformation of the brass skin was observed. Several test of this type were performed; in some of them the brass was bent during pulling because of an uneven substrate. Nevertheless there was no damage to the brass near the screws. Finally every second screw was removed and the test repeated. This time the material started yielding around several of the screws at a mean stress of 7500 psi = 1.05 kg^*/mm^2. Figure 6-3 shows a picture of the worst looking attachment hole after the screw was removed after this test. One sees the beginning of a tear. We conclude from this test that stresses of up to 3000 psi in the skin are allowable, if one wants a safety factor of 4-5.

washers get more and more compressed by the weight of the modules on top of it. In the end, the bottom plate is attached while the whole assembly is being compressed radially by a press attached to the jig. At the same time the readout cables are attached to the individual ground and sense absorber layers. Finally the skin, with holes predrilled and prepared in another jig, is screwed to the sides of the basic box. The unit is then tested for electrical insulation with HV, after which the preamplifiers are mounted, powered and the whole system tested again. If any repairs inside are needed, one of the skins can be removed. while the module is still being compressed from the outside.

7. Mounting of the modules.

A detailed description of the assembly of all the modules into the barrel is given in GEM-TN-903-309, so we can limit ourself to a brief summary and some discussion of items not mentioned in that note.

7.1 The inner hadronic modules.

The inner hadronic modules are in the end supported by the central washer and the cold cryostat headplate. These two components are mounted over the already assembled EM calorimeter while the assembly is in a vertical position. The assembly orientation is then changed so that the barrel is horizontal. There are splines mounted on both the central washer and on each of the headplates; these will position the keyways on each of the inner hadronic modules. On the central washer the splines are pre-positioned; but since one cannot guarantee the necessary tolerances between central washer and headplate, the splines on the headplate will have to be adjustable in position.

The inner hadronic modules are introduced into the assembly using a special manupulator. Once a module is in position, the locating pin holds it radially.

7.2 Feedthru ring.

Once all inner hadronic modules are installed, the bulkhead ring with the feedthrus is brought in and mounted. This ring is shown in Figure 7-1 Then one proceeds in making all the connections between the feedthrus and the EM amplifiers as well as the inner hadronic module amplifiers. At this stage one can test these units all the way up to and including the feedthrus. One also connects the cables from the feedthroughs to the outer hadronic modules at one end; the other end will be connected later.

7.3 Outer hadronic modules.

Now one installs the retaining ring for the outer hadronic modules shown in Figure 7-1. This ring has slots for the necessary cables, and has aligned splines mounted on it to accommodate the outer hadronic modules. The ring itself has to consist of several (probably 2) pieces so that it can be installed. The outer hadronic modules are then installed in the same way the inner modules were installed earlier.

We stress that once the ring for the outer hadronic modules is installed, there is no access to the feedthrus from the inside. It is therefore essential that the connections to all the inner modules be thoroughly tested before. Indeed, one should plan on mounting a small testing station near each of the feedthru positions onto the outside of the head plate so that the behavior of all amplifiers can be monitored throughout the assembly procedure - both before and after connecting to the feedthroughs. At a minimum, such a test station should be able to send a calibration pulse to an amplifier, and digitize the response. While such tests are performed at room temperature, they are adequate to predict the amplifier performance at the final cryogenic temperature.

8. Clearance space for the EM cables and feedthrus.

In our baseline design we are allocating 65 mm in z near each end of the barrel to the cables from the EM calorimeter. This allowance is less generous than it seems; nearly 2/3 of this is lost anyway to the required thickening of the headplate and the cylindrical stay around the EM calorimeter. Nevertheless, we still need to carefully study whether one can reduce this dead volume. One should note that hadrons going through there have encountered before this only the EM calorimeter and a small corner of the inner hadronic module. We need shower simulations studies for this region, and one might even contemplate inserting an extra massless gap there should it be shown that it will significantly improve the energy resolution. One also should create a mockup of a segment of this dead space in order to study how much of it one can save. Of course, for this one first has to specify exactly which cables will be used, and obtain samples so that one can test their bending characteristics.

Another dead space is the corner near the feedthrus. It also is shown in Figure 7-1. It seems unlikely that this space can be reduced in any significant way; this is the area where all the cables come together - signal, power, control and High voltage. Space has to be allocated so that one can make connections in the field. We also need a mockup of this area so that one can decide whether indeed all connections can be made safely.

9. Mother boards and cooling considerations.

The preamplifiers arrangement on the hadronic modules is much sparser than on the EM modules. An inner hadronic module will have ten motherboards, each with four such preamplifiers and the associated calibration circuitry. The location of these motherboards can be seen in Figure 6-1; Each will have a power consumption of approx 0.4 W, and each mother board will have a size of approx. 5 $cm \times 5$ cm. The outer hadronic module will have only eight units, each with two preamplifiers, and the power consumption per motherboard will also be only 0.2 W.

There is still some debate whether it is necessary to locally cool the motherboards with their preamplifiers. The present baseline specifies that the stay just outside the inner hadronic modules will carry coolant and thus these modules will be locally cooled. The outer hadronic modules are so close to the outer wall that special cooling is considered unnecessary. Of course, the main purpose of cooling is to prevent any gas bubbles of forming and entering the HV gap in any module; such a bubble would lead to immediate breakdown and loss of at least one amplifier.

10. Thermal contractions and tolerances.

We are using mostly brass as actual construction material, while the overall cryostat has an Aluminum structure. Luckily the contraction between room and $LN2$ temperature for the two is the same to 3 parts in 10^4. Thus even along the z-axis, where the modules are the longest, one expects a shift of only 1/2 mm. The tile planes will shrink as G-10 laterally (in z or ϕ), while they shrink nearly like lead or copper in the radial direction. The groundplanes shrink like copper, while the spacers are made of G-10. Thus the inside will generally shrink less than the outer dimension of the box, and our design accommodates these differences by keeping the absorber layers sliding inside a module; the Belleville washers keep then the krypton gaps well defined. Note, however, that since we are clipping the output current, the output signal is only a weak function of of the gap size.

11. Beam test of modules.

A major test of GEM calorimetry will start at Fermilab in the spring of 1995. The designated area is Mwest, where a previous experiment using LAr (E706) is being dismantled. This has the advantage that much of the necessary safety features (ODH tests, Cryo spill protection) already exist. We plan to dismantle the Gantry which houses the present E706 cryostat, and replace it with a cryostat on a transporter which can be rotated, raised and tilted such the incident beam simulates particles emanating from the interaction region and hitting different parts of the cryostat[2]. For this first beam test we plan to provide a minimum of 3 inner and 3 outer hadronic barrel modules. Other groups (BNL, Seattle, Columbia) plan to provide barrel EM modules and endcap modules (both EM and hadronic). Figure 13-1 shows a lateral view of the barrel modules inside the cryostat; the cryostat itself is large enough to accommodate also an equivalent sample of Endcap modules, as well as full length barrel EM modules. If one wants to study the behavior of the barrel calorimeter near the central washer, one must add 6 more barrel hadronic modules to cover the other side of the washer. The cash flow will determine whether this can be achieved in the 1995 run, or has to be postponed to a later time.

Footnotes:

[1] The compensation is partial because the signal from a single cell travels on the cable in both directions: The half moving away from the preamplifier is reflected at the far end and arrives later. Furthermore, some of the signal will also be reflected on the amplifier end if the amplifier input impedance is not an exact match to the cable impedance.

[2] The cryostat is being designed by SSCL, the actual transporter by Rochester

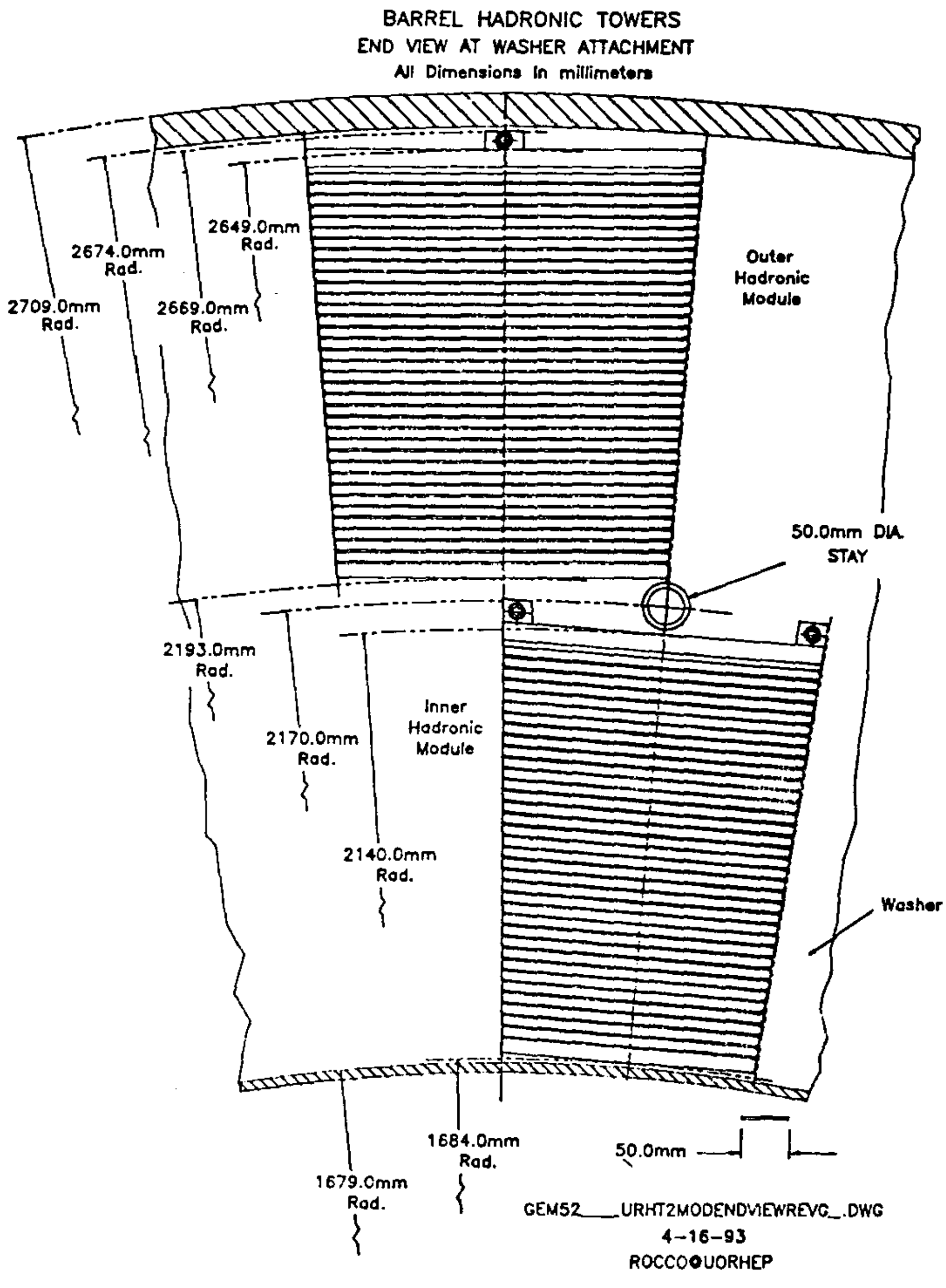

Figure 2-1: A cross sections of the barrel hadronic modules (End view)

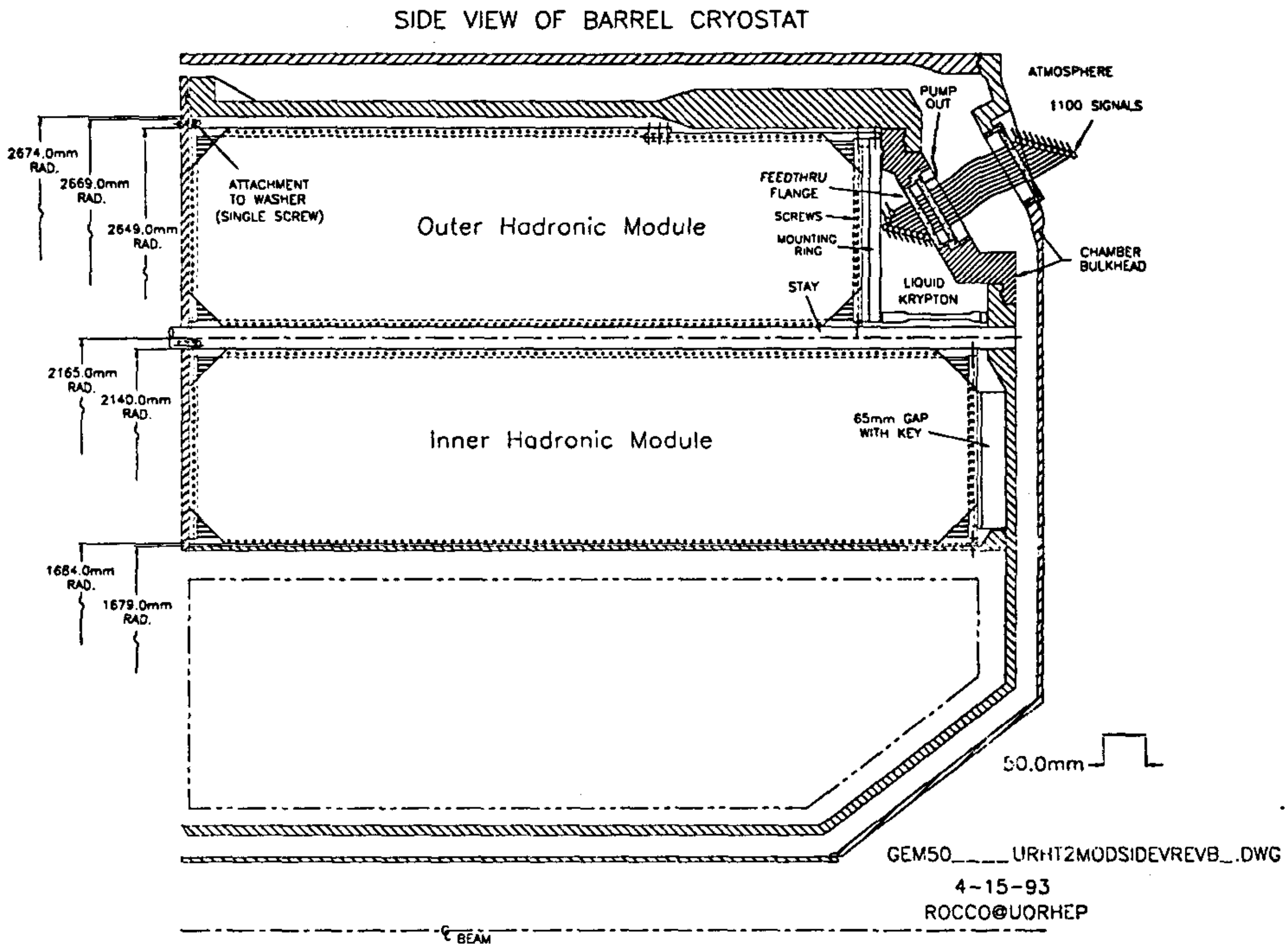

Figure 2-2: The hadronic modules inside the barrel cryostat (Side view)

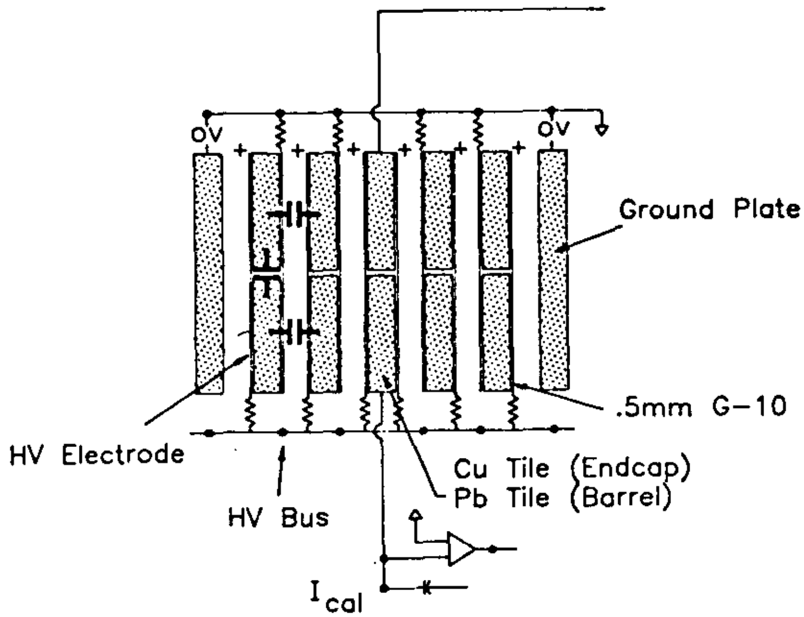

Figure 3-1: The chosen cell structure using a Electrostatic Transformer of 3:1.

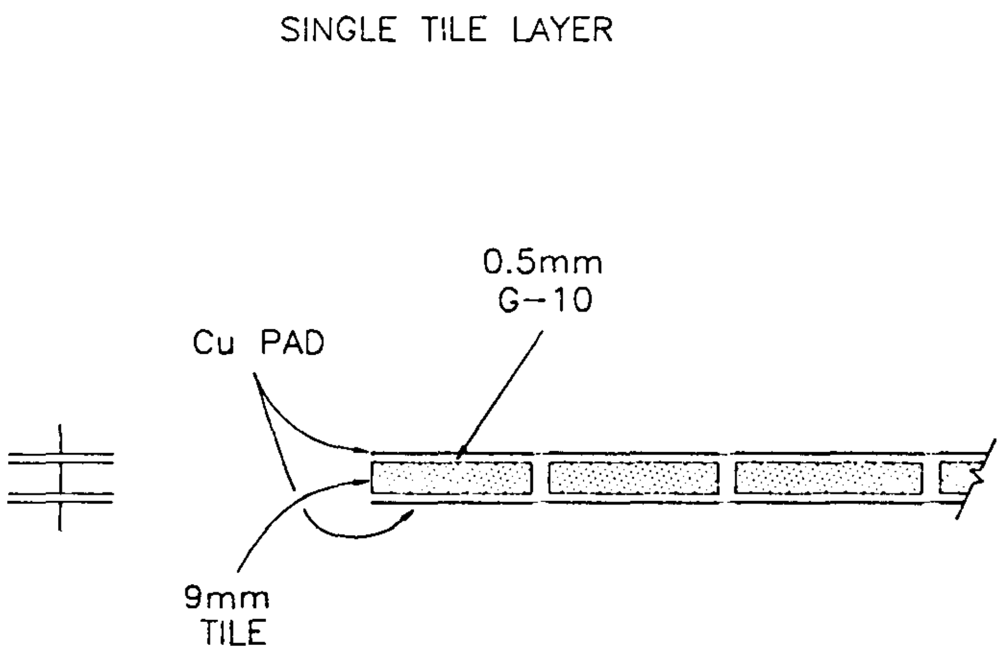

Figure 3-2: A Tile Absorber layer, with the *G*-10 boards and pads; on the side we are showing the electric equivalent circuit.

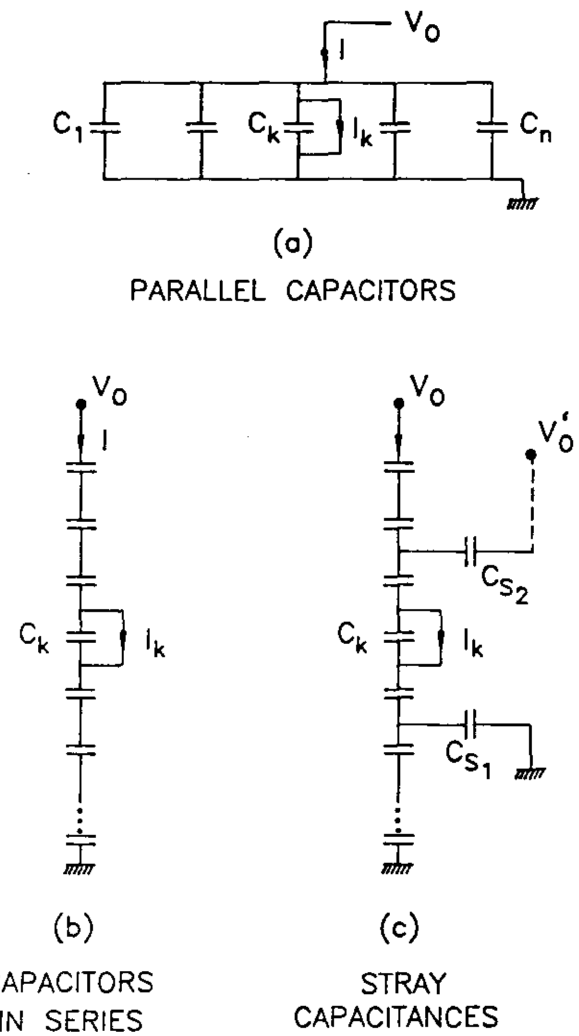

Figure 3-3: Sensing the current in one of many capacitors at the "source" V_o.

a. Parallel Capacitors

b. Capacitors in Series

c. Stray Capacitances

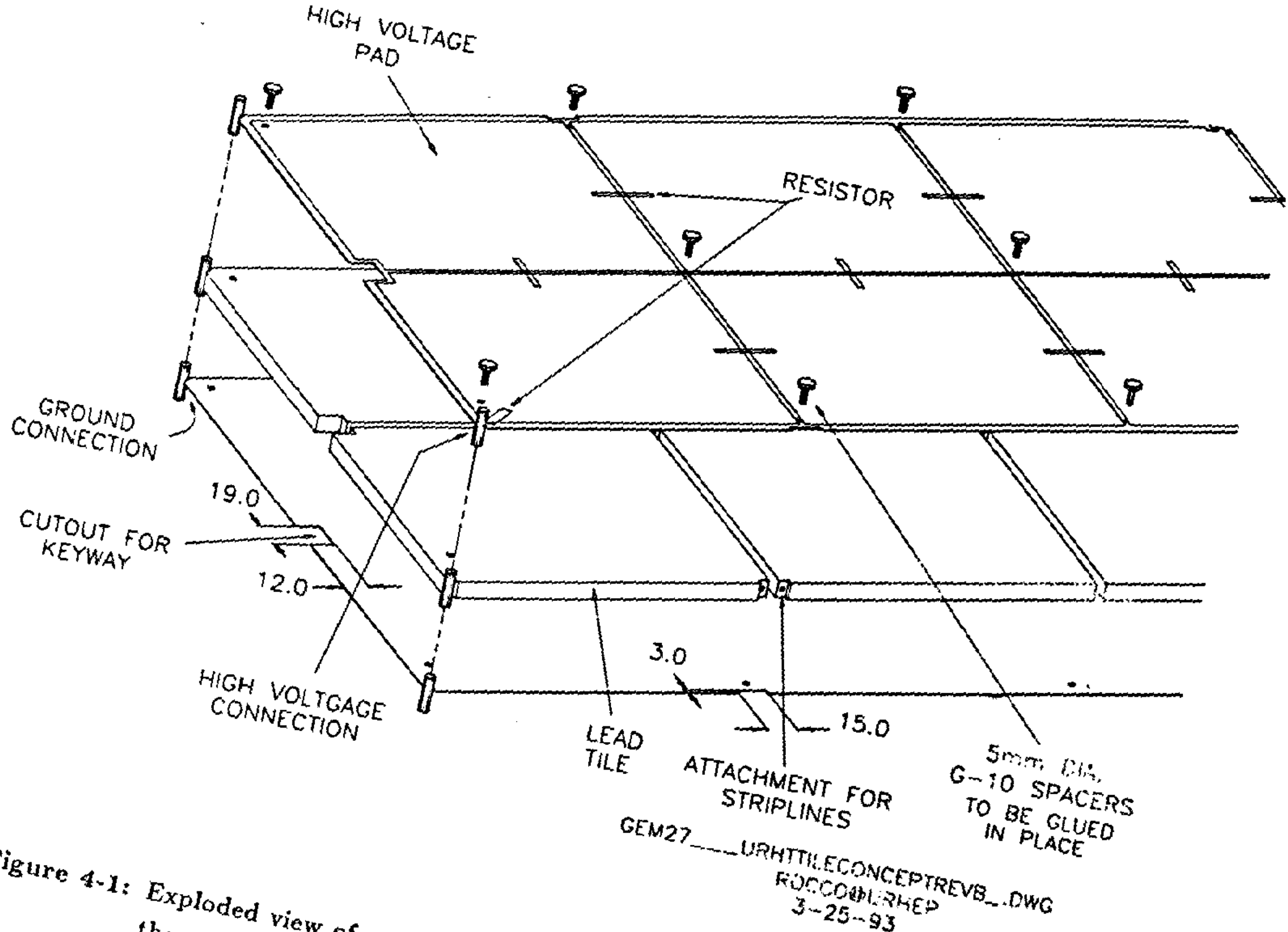

Figure 4-1: Exploded view of one end of a tile absorber layer, showing spacers, as well as the notches for cable connections and keyways for atttaching the layer to the endplates

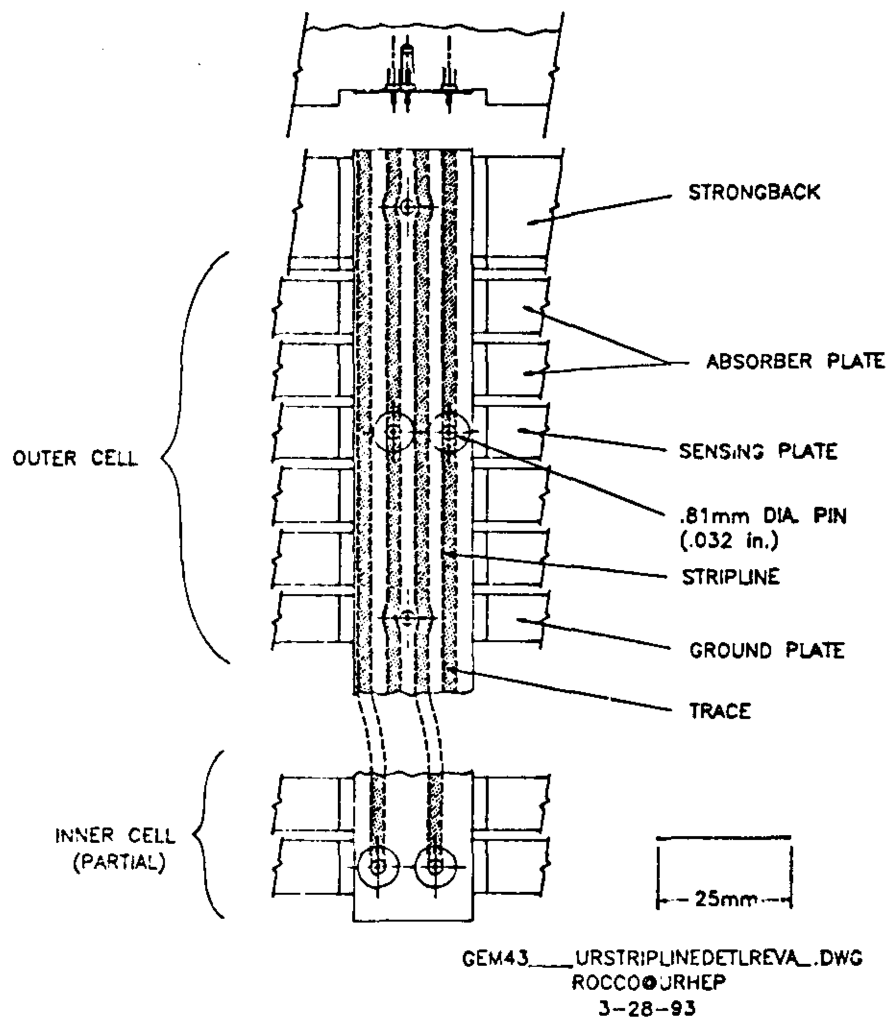

Figure 4-2: Connection to the readout cable which connects tiles to the preamplifier

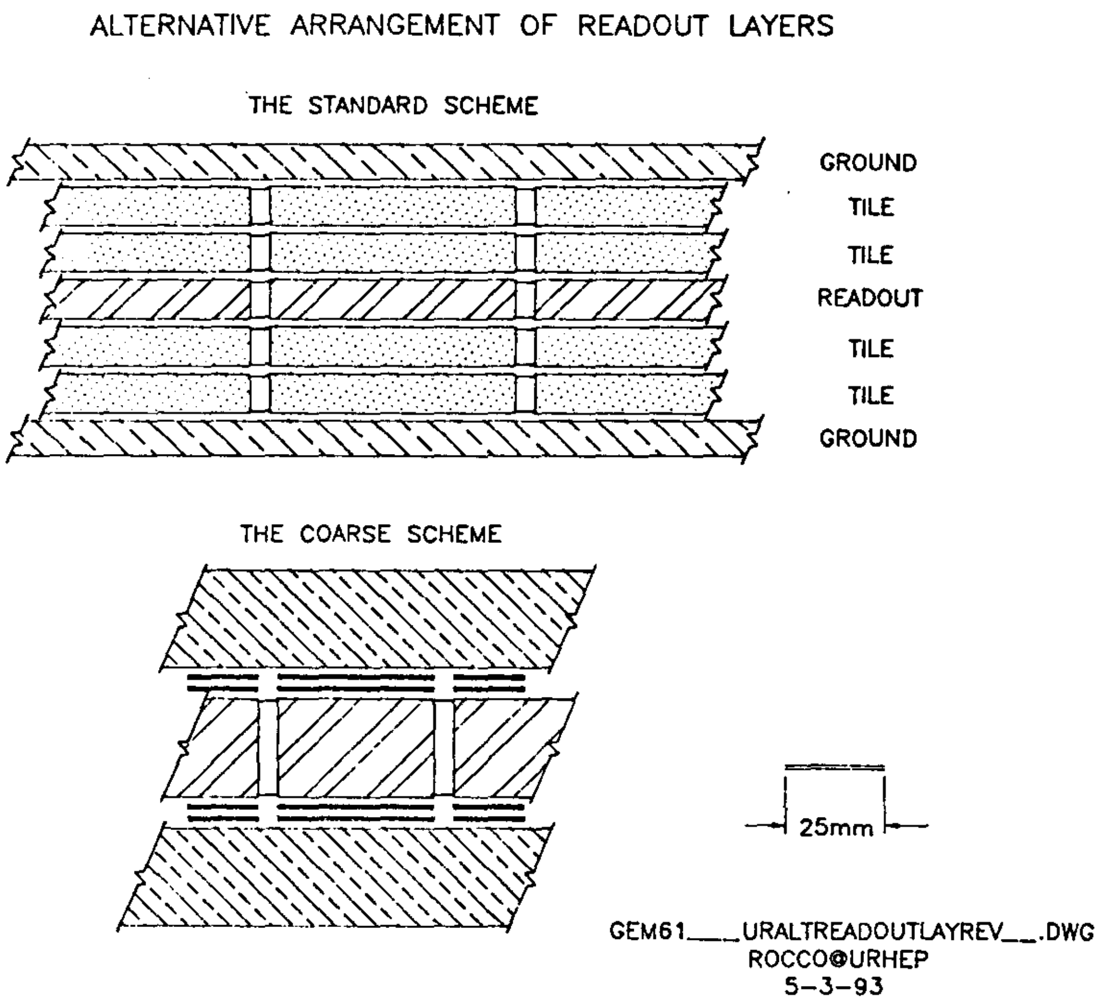

Figure 4-3: Comparison of the Standard absorber pattern to a coarser but possibly cheaper pattern where all the absorber is concentrated in the ground plane and in the sense tile plane.

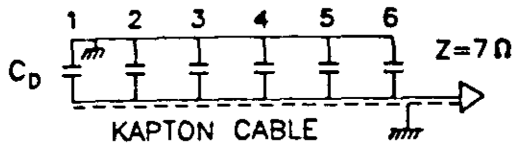

Figure 5-1: Equivalent circuit diagram for reading out six cells. We assume a perfect termination of the cable at the amplifier input.

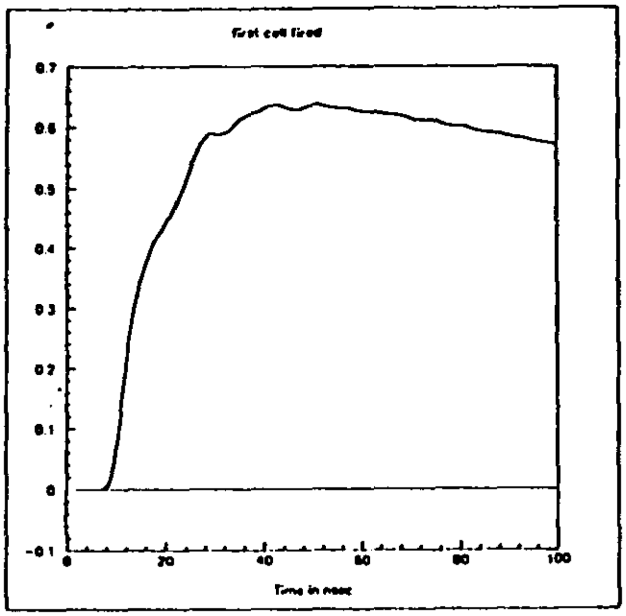

(a)

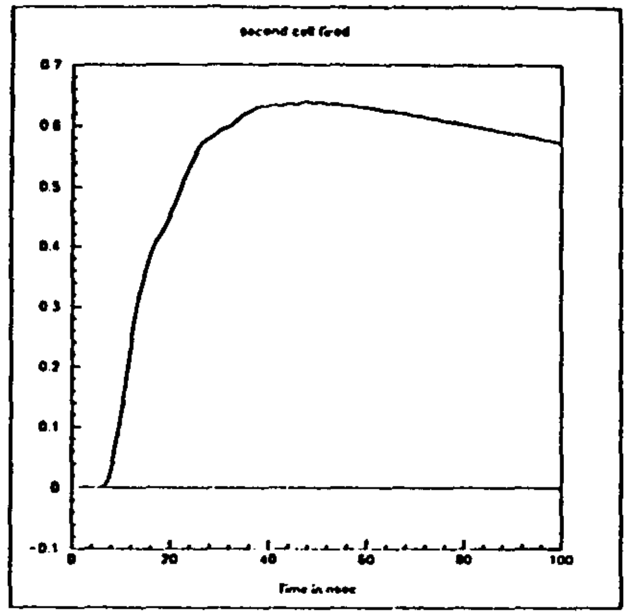

(b)

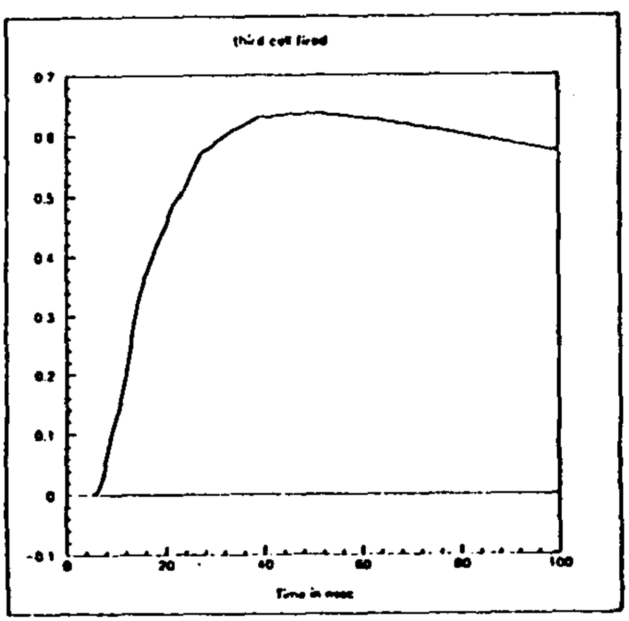

(c)

Figure 5-2:

When a pulsed current is generated in one cell only, the output of the amplifier shows a slightly different shape. The values chosen are typical for the outer hadronic layer where all six cells are read out by a single amplifier.

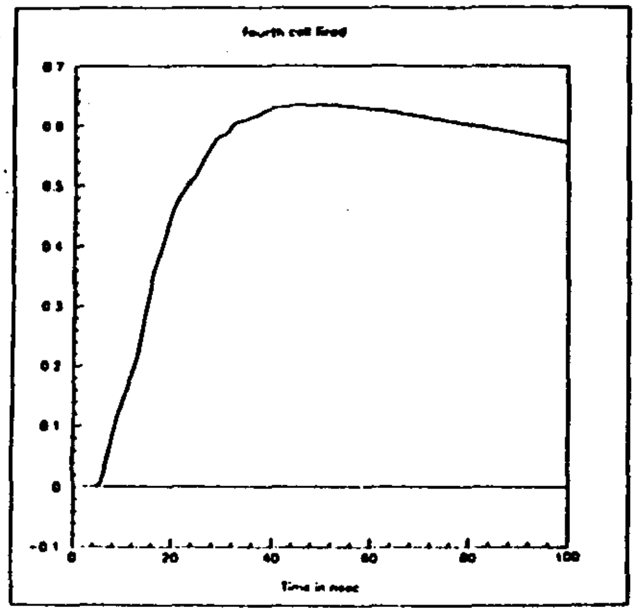

(d)

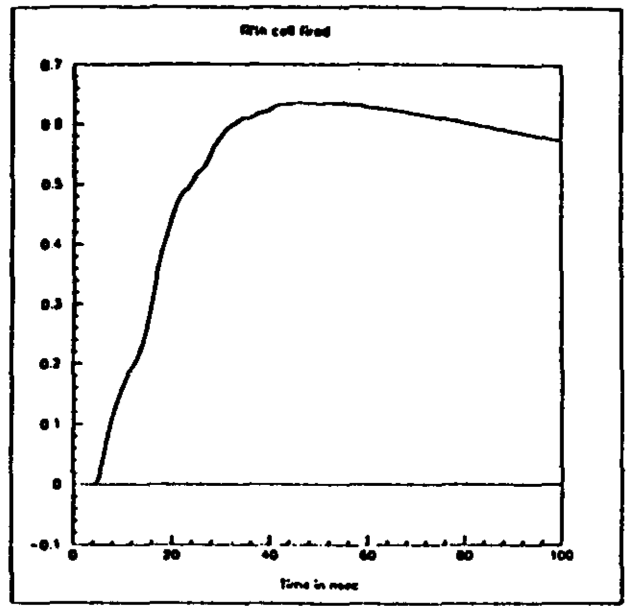

(e)

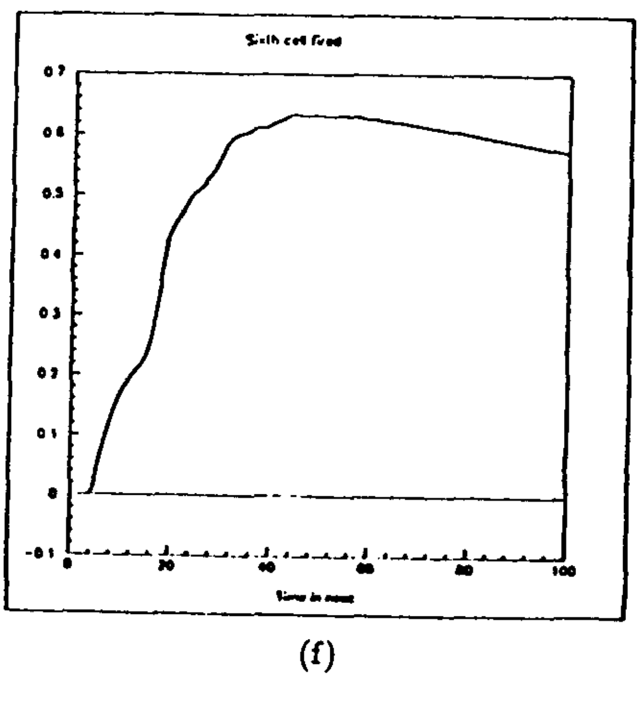

(f)

Figure 5-2:

When a pulsed current is generated in one cell only, the output of the amplifier shows a slightly different shape. The values chosen are typical for the outer hadronic layer where all six cells are read out by a single amplifier.

SINGLE SIGNAL CONNECTION

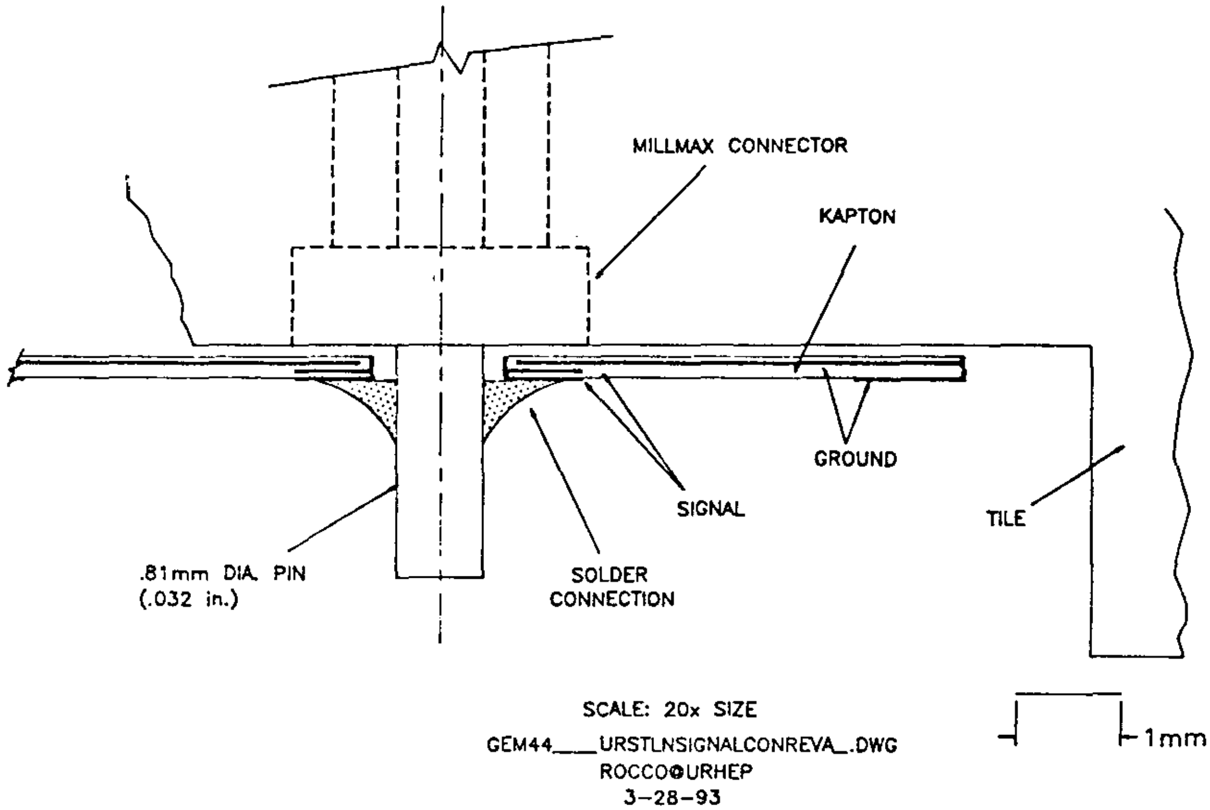

Figure 5-3: The Readout cable pattern around the pin which connects it to a tile.

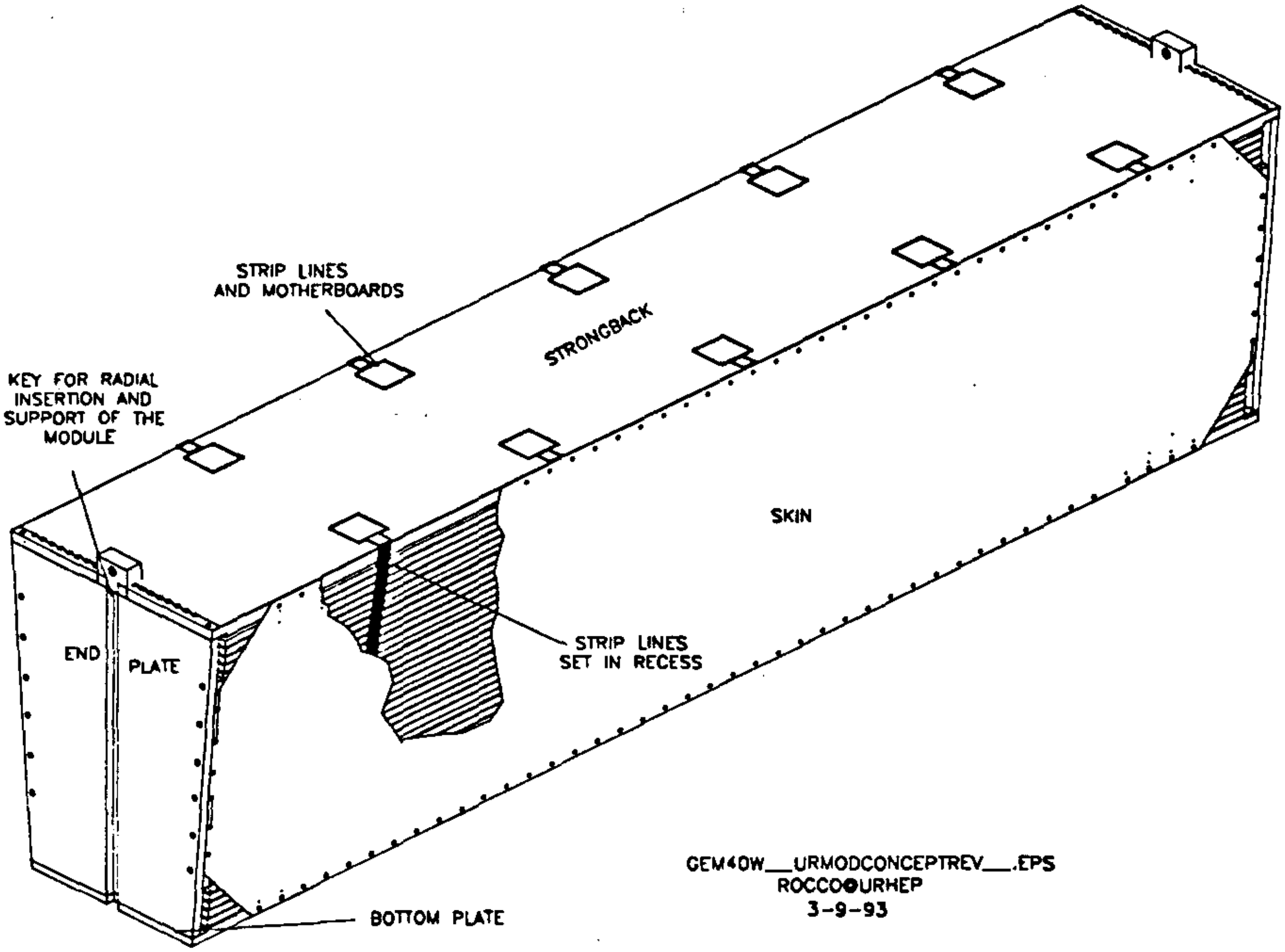

Figure 6-1: An assembled inner hadronic module, with identification of the individual elements.

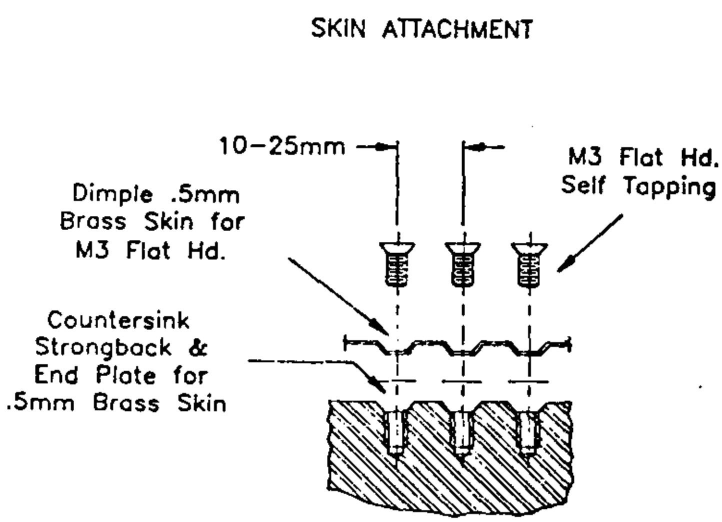

Figure 6-2: Fastening the skin to the Strongback, Endplate or Bottom plate.

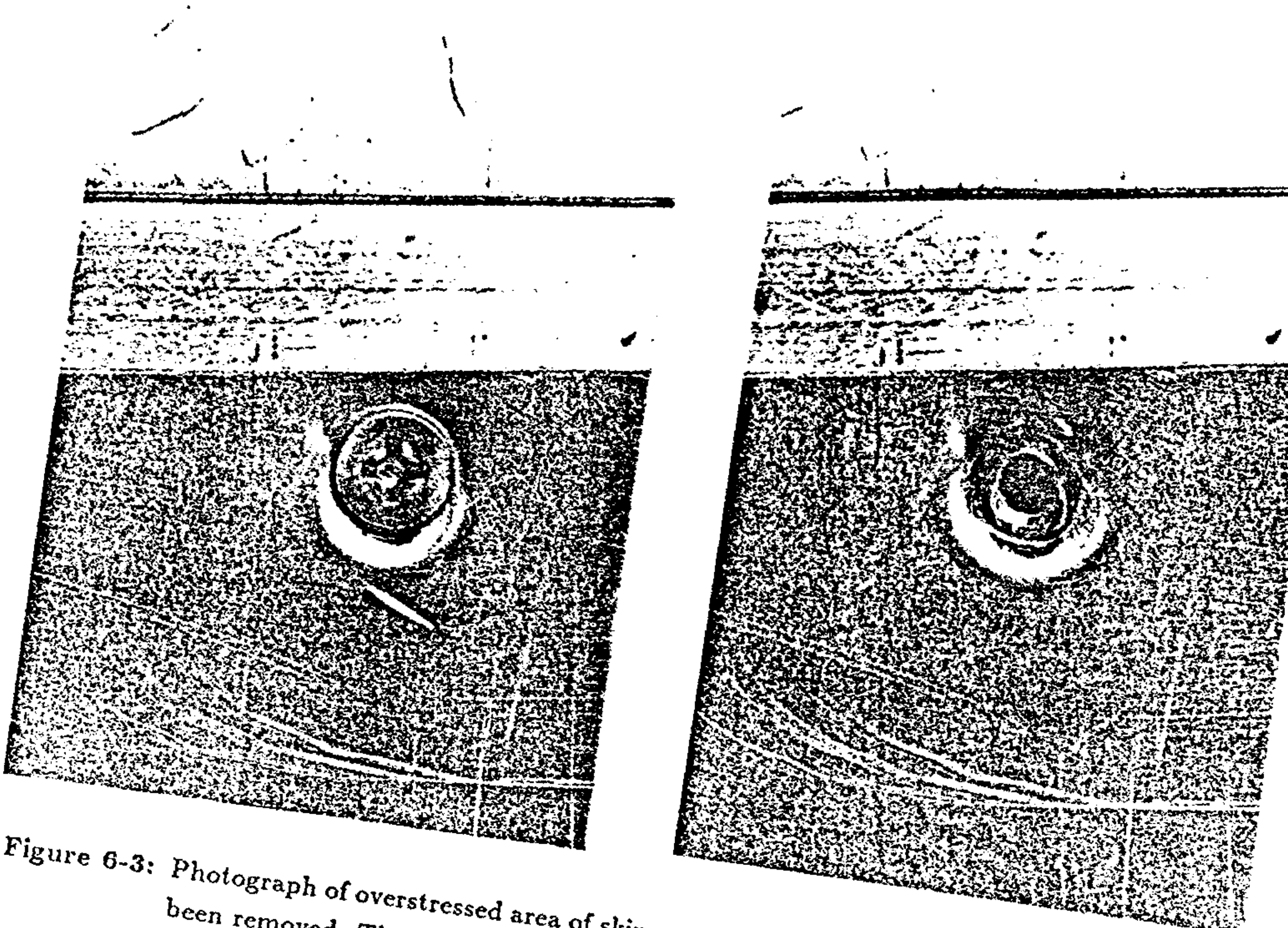

Figure 6-3: Photograph of overstressed area of skin; on left the screw is still in, on the right it has been removed. This is the worst of 12 attachment points used during this test where the material was on purpose stretched beyond its yield point.

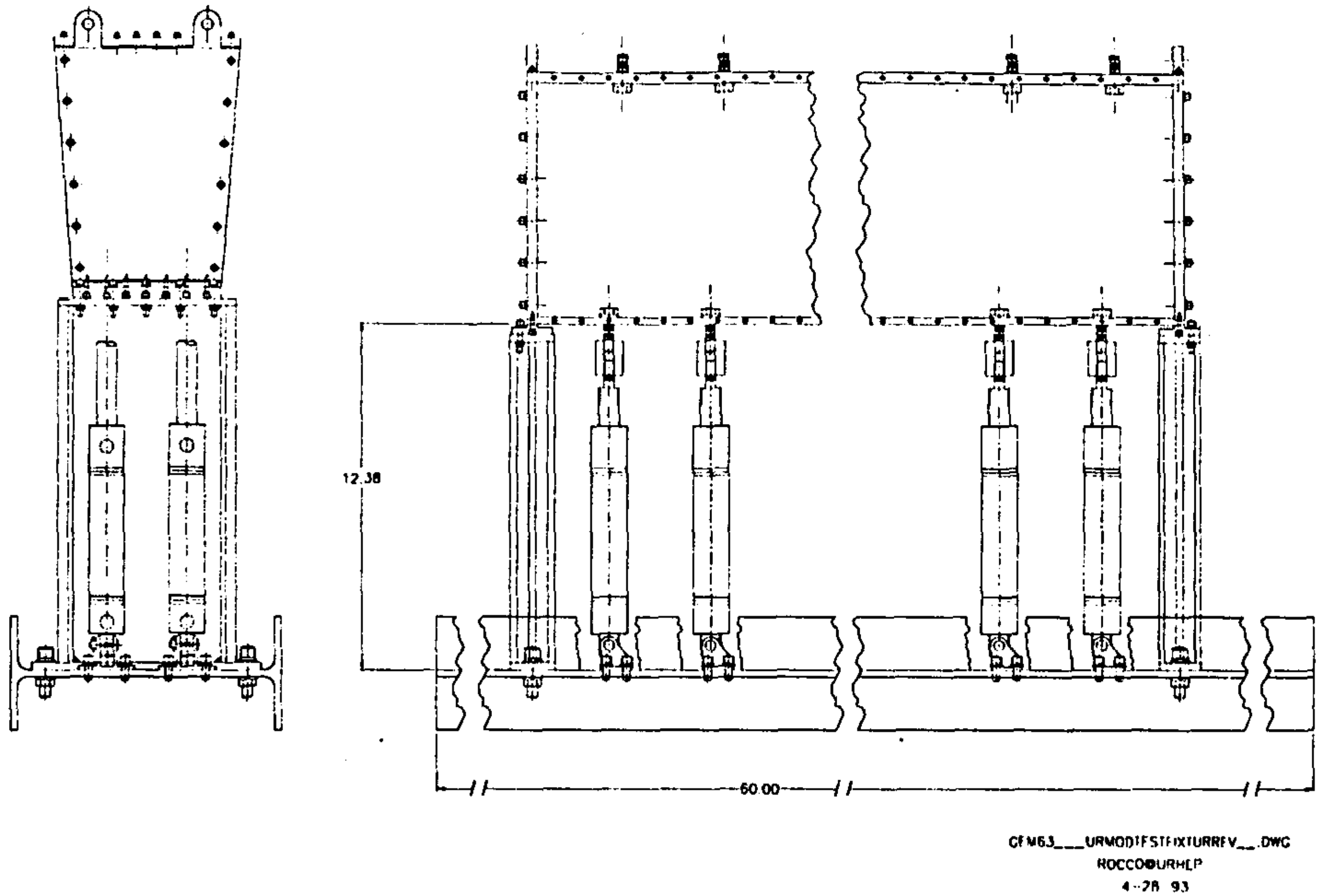

Figure 6-4: Drawing of the teststand to test behavior of modules under loads.

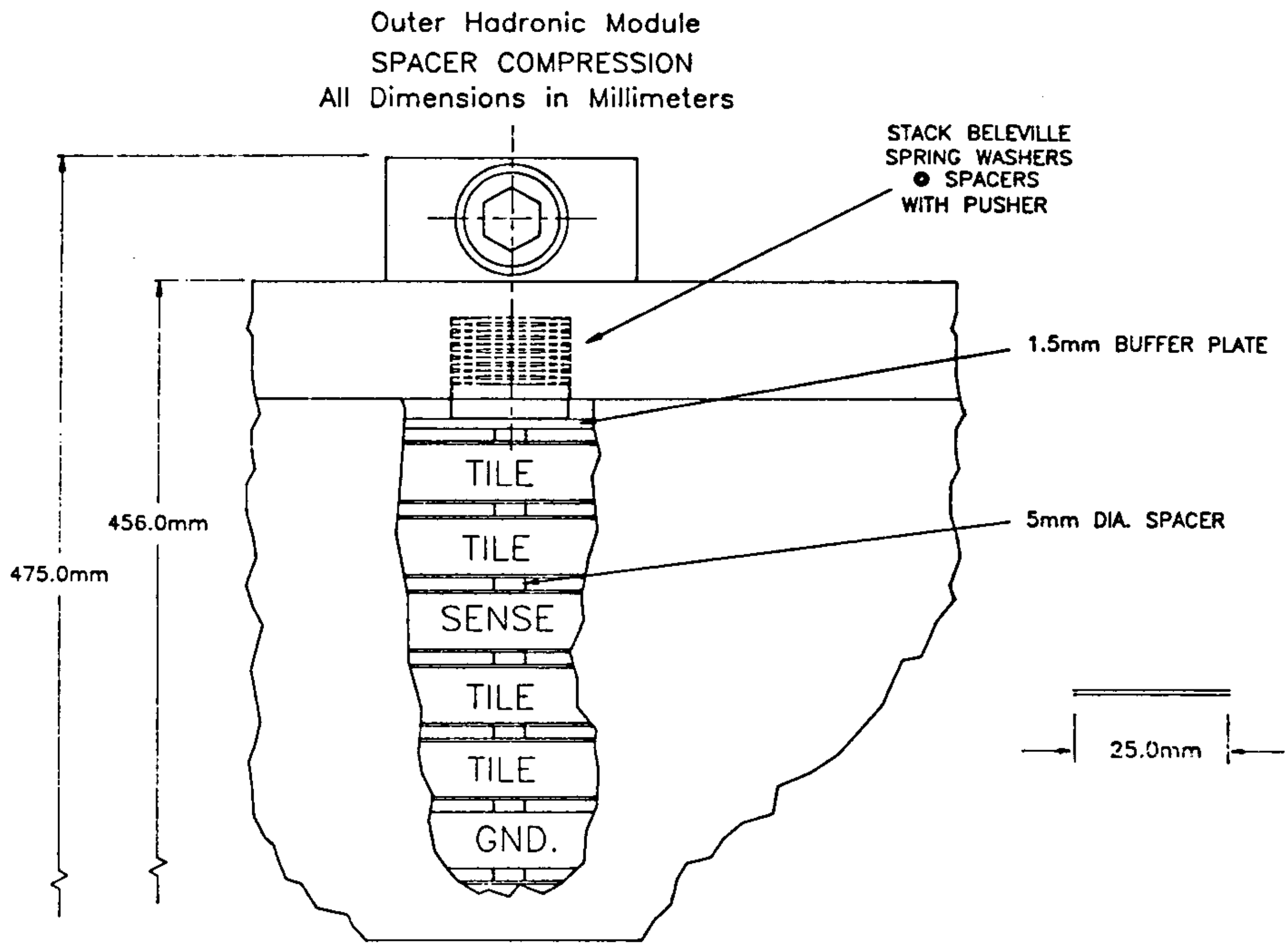

Figure 6-5: Compression of a module stack. A set of Belleville washers pushes a plunger which acts through a thin buffer plate directly on the spacers.

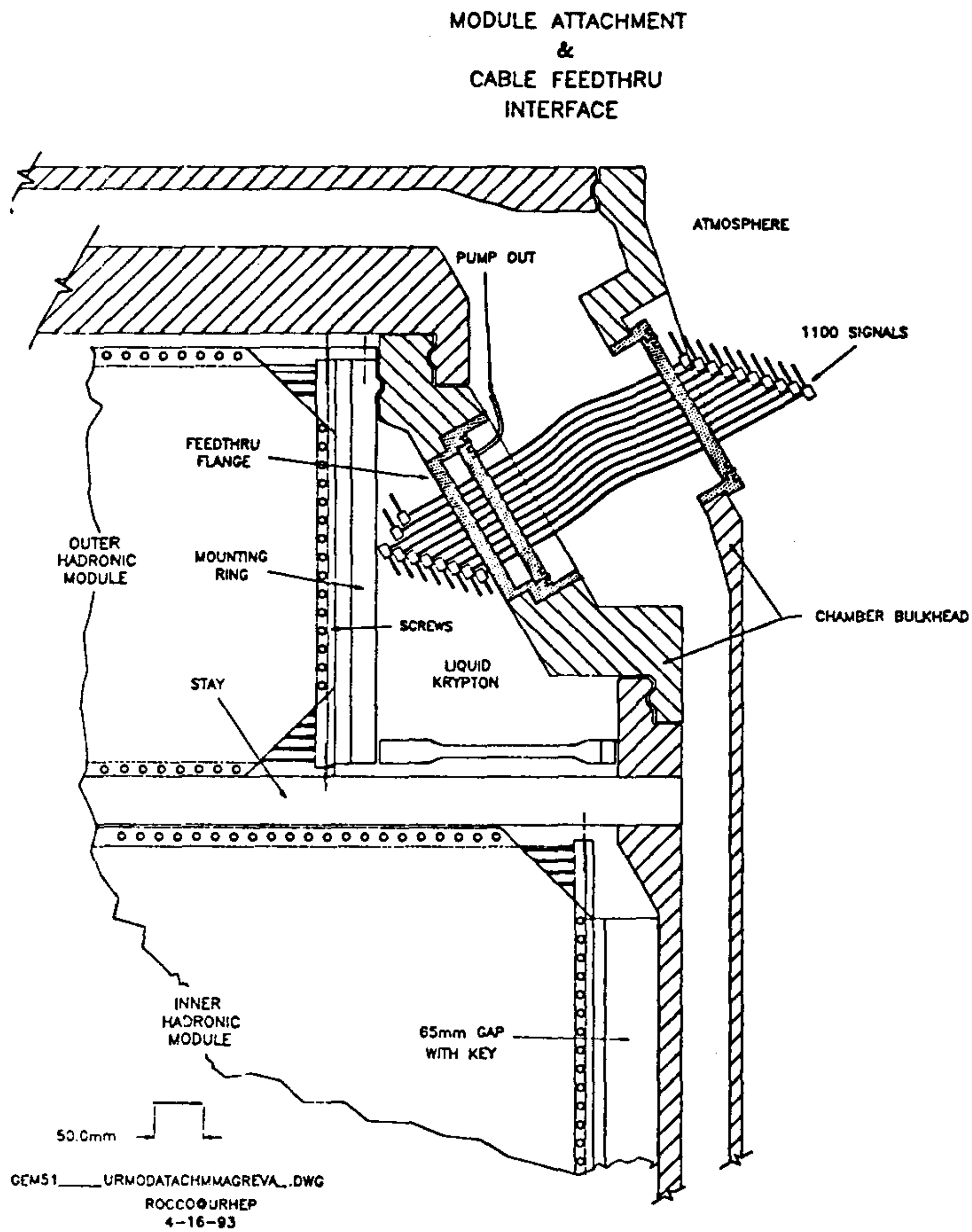

Figure 7-1: Detail of inner barrel cryostat near the feedthrus, showing the ring on which the outer hadronic modules will be mounted.

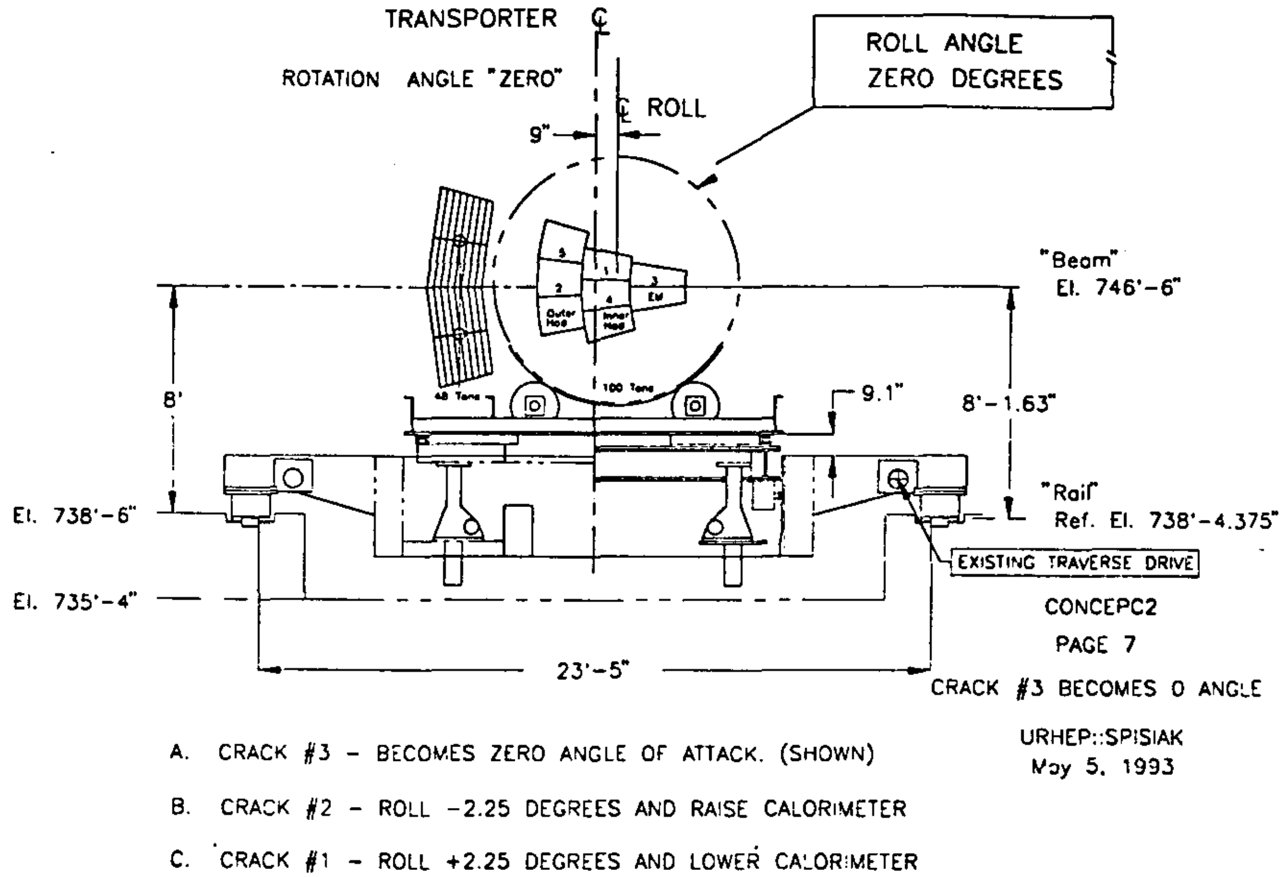

Figure 13-1: The test beam cryostat and its transporter. Two EM barrel modules, and three each of inner and outer hadronic modules are shown. Behind it one sees the scintillating warm calorimeter layer. This setup is planned for the MWEST area at Fermilab.